Optimizing Ionic Transport in Metal-Supported Solid Oxide Fuel Cells: Influence of Electrolyte Thickness

M. Kamal Warshi , Zheng Dao Jin , Sang Eun Lee , Kyoung-jin Lee , Hee Jung Park *

Posted Date: 17 March 2026

doi: 10.20944/preprints202603.1306.v1

Keywords: metal-supported SOFC; electrolyte thickness; tape casting; co-sintering

 doi:10.20944/preprints202603.1306.v1

Article

Optimizing Ionic Transport in Metal-Supported Solid Oxide Fuel Cells: Influence of Electrolyte Thickness

M. Kamal Warshi [1,2], Zheng Dao Jin [2], Sang Eun Lee [2], Kyoung-jin Lee [3] and Hee Jung Park [1,2,*]

[1] Hydrogen Research Center, Dankook University, Dandae-ro 119, Dongnam-gu, Cheonan 31116, Korea
[2] Department of Materials Science and Engineering, Dankook University, Dandae-ro 119, Dongnam-gu, Cheonan 31116, Korea
[3] Wonik Materials, Jangdae-gil 20, Ochang, Chungju 28219, Korea
* Correspondence: parkjang@dankook.ac.kr

Abstract

Metal-supported solid oxide fuel cells (MS-SOFCs) represent a promising advancement for intermediate-temperature energy conversion applications due to their enhanced mechanical robustness and rapid startup capabilities. This investigation systematically evaluates the correlation between yttria-stabilized zirconia (8YSZ) electrolyte thickness and electrochemical performance in Ni-Fe supported architectures. Three distinct cells featuring YSZ electrolyte thicknesses of 7.05, 14.2, and 21.2 μm were fabricated via tape casting and co-sintering at 1350°C, maintaining identical Ni-Fe support (280 μm) and Ni-YSZ anode (22 μm) thicknesses. Electrochemical characterizations revealed a clear inverse relationship between electrolyte thickness and cell performance. The cell with the thinnest electrolyte (7.05 μm) achieved the highest power density of 0.32 W/cm² at 800°C, representing a 4.6-fold improvement compared to the thickest variant (21.2 μm). Electrochemical Impedance Spectroscopy and Distribution of Relaxation Times analysis confirmed that ohmic resistance dominated the total cell impedance, scaling linearly with electrolyte thickness while electrode kinetics remained consistent. This study establishes that thin YSZ electrolytes (≤8 μm) maximize MS-SOFC performance while maintaining structural integrity through co-sintering fabrication, providing an essential design for high-performance metal-supported fuel cell development.

Keywords: metal-supported SOFC; electrolyte thickness; tape casting; co-sintering

Introduction

Solid oxide fuel cells (SOFCs) represent one of the most promising electrochemical energy conversion technologies due to their high efficiency, fuel flexibility, and potential for combined power applications [5,22,23,35]. However, the broader commercialization of SOFCs has been hindered by challenges related to mechanical durability, thermal cycling resistance, and high operating temperatures [13,21,26,27]. Traditional electrolyte-supported and anode-supported SOFC designs, while demonstrating excellent electrochemical performance, suffer from inherent brittleness and susceptibility to thermal shock, particularly during startup and shutdown cycles [7,29].

Metal-supported solid oxide fuel cells (MS-SOFCs) have emerged as a compelling alternative that addresses many of these limitations. The incorporation of a metallic support structure provides several key advantages: enhanced mechanical robustness, improved thermal shock resistance, rapid startup capabilities due to lower thermal mass, and the potential for operation at intermediate temperatures [12,32]. These characteristics make MS-SOFCs particularly attractive for automotive, supplementary power unit, and distributed energy applications where durability and rapid response are critical requirements [8,38].

 doi:10.20944/preprints202603.1306.v1

The development of MS-SOFCs, however, presents unique challenges in fabrication and design. The selection of appropriate metal support materials must balance mechanical properties, thermal expansion compatibility, and electrochemical stability under SOFC operating conditions. Nickel-iron (Ni-Fe) alloys have shown promise as support materials due to their favorable thermal expansion coefficients, good mechanical properties, and compatibility with conventional solid oxide fuel cell (SOFC) processing temperatures [4,14,17,22,34]. Additionally, the fabrication of thin, dense electrolyte layers on metal supports requires careful optimization of processing parameters to ensure gas-tight sealing while minimizing ohmic losses [3,8].

Among the various design parameters that affect MS-SOFC performance, the electrolyte thickness plays a crucial role in determining the overall cell efficiency [15]. The electrolyte layer must be sufficiently thick to prevent gas crossover between fuel and oxidant compartments while maintaining mechanical integrity. Conversely, reducing electrolyte thickness decreases ohmic resistance, thereby improving power density and efficiency [6,9,18]. This trade-off between gas-tightness and ionic conductivity necessitates careful optimization of electrolyte thickness for each specific cell design and operating condition.

Yttria-stabilized zirconia (YSZ) remains the most widely used electrolyte material in SOFC applications due to its excellent ionic conductivity, chemical stability, and well-established processing techniques [36,37]. At intermediate temperatures (500-700°C), YSZ exhibits ionic conductivities of 1.1×10^{-3} S/cm at 500°C, which, while lower than advanced alternatives like gadolinium-doped ceria (GDC) or scandia-stabilized zirconia (ScSZ), remains viable for thin-film applications [25,28,39]. However, fabricating ultra-thin YSZ layers on metal supports poses significant challenges due to thermal expansion mismatches, sintering behavior, and interfacial adhesion. Co-sintering approaches, where multiple layers are simultaneously processed, offer potential solutions to these fabrication challenges by promoting better interfacial bonding and reducing processing-induced stresses [4,12].

Recent advances in tape casting and lamination techniques have enabled the fabrication of multi-layer MS-SOFC structures with precise thickness control and excellent layer-to-layer adhesion [4]. These processing methods allow for systematic investigation of individual layer thickness effects on overall cell performance, providing valuable insights for design optimization [30].

Despite the growing interest in MS-SOFCs, systematic studies investigating the optimal electrolyte thickness for Ni-Fe-supported cells remain limited. Most previous work has focused on proof-of-concept demonstrations or comparative studies between different support materials, with less attention given to the detailed optimization of individual layer thicknesses [32]. Furthermore, the relationship between electrolyte thickness and performance in MS-SOFCs may differ significantly from conventional cell designs due to the unique thermal and mechanical constraints imposed by the metal support [38].

The objective of this study is to systematically investigate the effect of YSZ electrolyte thickness on the electrochemical performance of Ni-Fe-supported SOFCs fabricated using co-sintering techniques. By maintaining consistent support and anode thicknesses while varying only the electrolyte thickness, we aim to establish clear design guidelines for optimizing MS-SOFC performance. The study employs a combination of electrochemical characterization, impedance spectroscopy, and microstructural analysis to identify the optimal electrolyte thickness that maximizes power density while maintaining structural integrity and gas-tightness.

2. Experimental Details

The metal-supported solid oxide cells (MS-SOCs) were fabricated using a slurry-based tape casting process. The fabrication sequence comprised slurry preparation, tape casting, lamination, cutting, and co-sintering at 1350°C for 3 hours. Three distinct layers were prepared: the support layer (Ni-Fe), the anode layer (Ni-YSZ), and the electrolyte layer (YSZ). The support layer was prepared by mixing commercially available NiO and Fe_2O_3 powders (Kceracell, Korea) in a 1:1 weight ratio.

 doi:10.20944/preprints202603.1306.v1

The anode layer was composed of NiO and YSZ powders combined in a 6:4 weight ratio (Kceracell, Korea). The electrolyte layer consisted of YSZ containing 8 mol% Y_2O_3 and 92% ZrO_2 (Tosoh, Japan).

The ceramic powders for all layers were dispersed separately in a solvent mixture of propyl acetate and ethanol. To ensure uniformity, commercial dispersants (BYK, Germany) were added. Polymethyl methacrylate PMMA (Sunjin Chemical, Korea) was added as a pore former to the anode and support layers. The slurry was ball-milled for 24 hours to achieve a homogeneous mixture, after which organic binders and plasticizers were incorporated. The slurry was then ball-milled for an additional 24 hours to ensure proper dispersion and texture, making it suitable for tape casting. The resulting slurry was then degassed and cast to form flexible green tape. The support, anode, and electrolyte layers were laminated using a hot roll press. The laminated tape was then laser-cut into 23 mm discs. The green tap discs were heated in a furnace in an air atmosphere. Initially, the temperature was raised at 1 °C/min up to 550 °C and held for an hour to burn out the organic additives and PMMA. Afterward, the temperature was increased at a rate of 3 °C/min to 1350 °C, where it was maintained for 3 hours to form a highly dense electrolyte layer [12].

Figure 1a,b illustrate the final structure and complete fabrication process of the NiFe supported SOFC cells investigated in this study. The cell architecture (Figure 1a) consists of a NiFe PMMA (10 µm, 15% porosity) metal support serving as the structural backbone, followed by a Ni-YSZ(60:40)-PMMA (3 µm, 15%) anode layer, a dense YSZ electrolyte layer of varying thickness (7.05, 14.2, and 21.2 µm), and a screen-printed LSCF cathode with platinum current collectors on both sides.

The fabrication process, Figure 1b, begins with individual tape casting of each functional layer using green tape technology. The support layer uses NiO-Fe_2O_3 composition, the anode employs NiO-YSZ, and the electrolyte consists of pure YSZ. After tape casting, the green tapes are laminated together and cut into circular samples. The co-sintering process simultaneously densifies the support, anode, and electrolyte layers while burning out the organic binders (PMMA), resulting in the final sintered cells (Cell_1, Cell_2, Cell_3) with different electrolyte thicknesses. This co-sintering approach ensures excellent interfacial adhesion between layers and enables precise control of electrolyte layer thickness while maintaining consistent support and anode dimensions across all samples. The use of PMMA as a pore former in both the support and anode layers creates the necessary porosity for gas transport, while the electrolyte remains dense to prevent gas crossover.

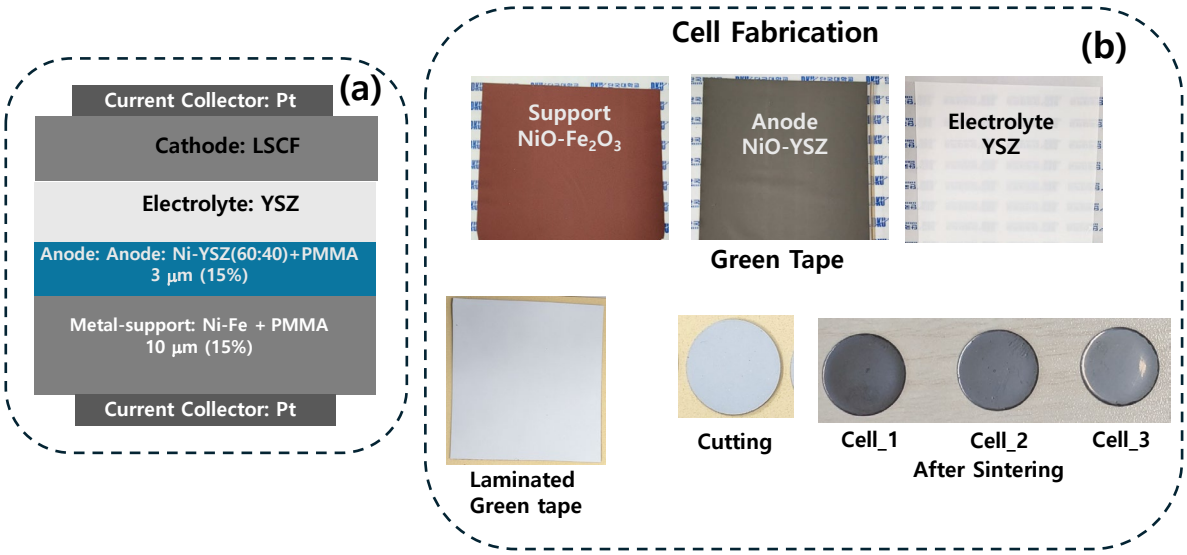

Figure 1. Schematic illustration of NiFe-supported SOFC structure and fabrication process. (a) Cross-sectional view of the multilayer cell architecture showing material composition. (b) Fabrication sequence from tape casting of individual green tapes through lamination, cutting, and co-sintering to produce cells with varying electrolyte thickness.

 doi:10.20944/preprints202603.1306.v1

The electrochemical performance of the MS-SOCs was evaluated in solid oxide fuel cell (SOFC) operation mode using current-voltage (I-V) measurements and electrochemical impedance spectroscopy (EIS). Disc-shaped cells were sealed into a test fixture using ceramic glass sealant. Platinum paste and mesh were applied as current collectors on both the anode and cathode sides. During SOFC testing, the anode was supplied with a gas mixture comprising dry hydrogen (H_2, 90 sccm) and nitrogen (N_2, 10 sccm) at a total flow rate of 100 sccm, while the cathode was exposed to air at 100 sccm. Current-voltage characteristics were measured using a galvanostat and impedance analyzer (Wonatech, Zive MP-2). EIS measurements were conducted under open-circuit conditions over a frequency range of 0.1 Hz to 2 MHz using a logarithmic frequency-sweep mode with an amplitude of 10 mV.

3. Results and Discussions

Figure 2 presents cross-sectional SEM micrographs of the three fabricated NiFe-supported SOFC cells, demonstrating successful co-sintering and consistent microstructure across different electrolyte thicknesses. All three cells exhibit well-defined, distinct layers with clear interfaces between the support, anode, electrolyte, and cathode components. The layered architecture is maintained consistently across all samples, confirming the effectiveness of the tape casting and co-sintering approach for producing high-quality MS-SOFC structures.

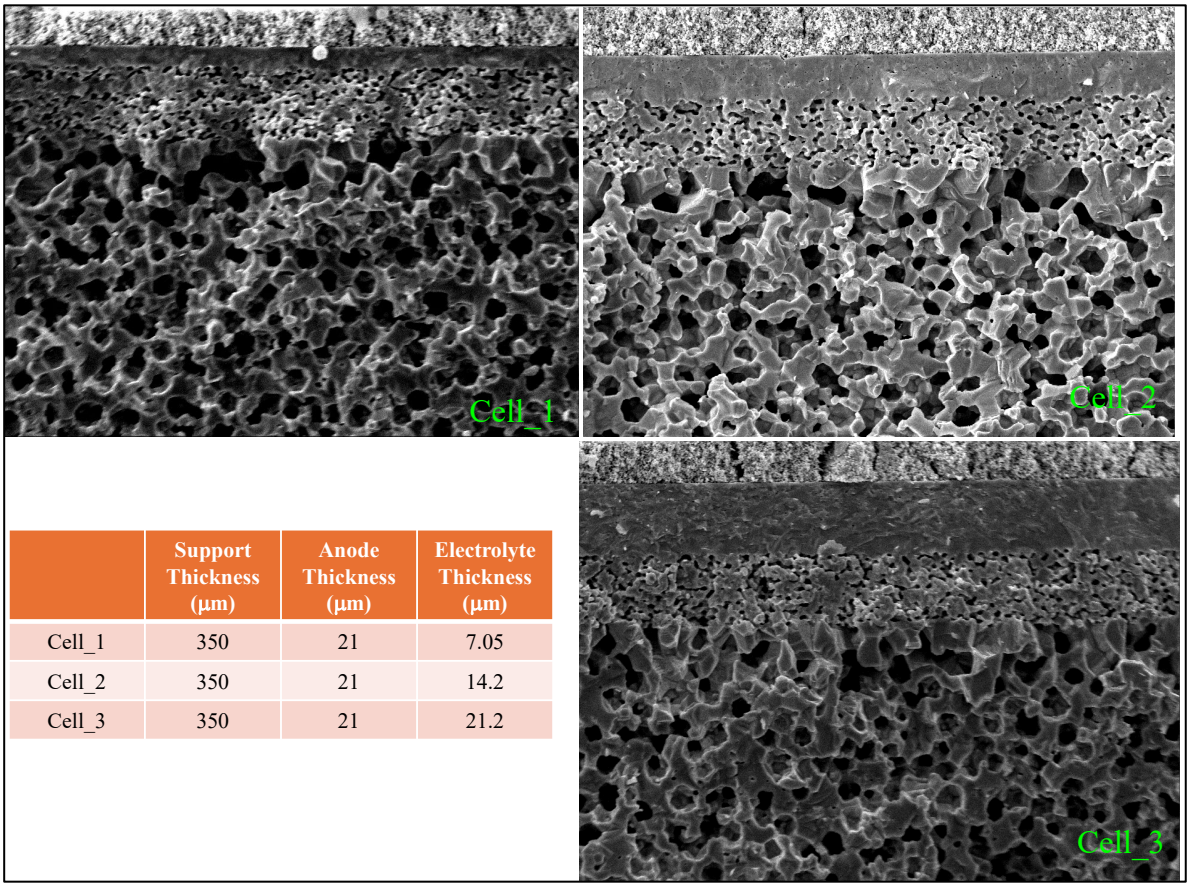

	Support Thickness (μm)	Anode Thickness (μm)	Electrolyte Thickness (μm)
Cell_1	350	21	7.05
Cell_2	350	21	14.2
Cell_3	350	21	21.2

Figure 2. Cross-sectional SEM micrographs of NiFe-supported SOFC cells with varying YSZ electrolyte thickness. Cell_1 (7.05 μm), Cell_2 (14.2 μm), and Cell_3 (21.2 μm) showing the complete multilayer structure: NiFe support, Ni-YSZ anode, YSZ electrolyte, and screen-printed LSCF cathode. The table summarizes the measured layer thicknesses for each cell.

The NiFe support shows uniform porosity with interconnected pore networks essential for gas transport. The pore structure appears consistent across all cells, with pore sizes ranging from 8 to 10

 doi:10.20944/preprints202603.1306.v1

microns, created by the burnout of PMMA pore former during sintering. The support thickness is maintained at 280 μm for all samples.

The Ni-YSZ anode layer shows appropriate porosity for fuel transport while maintaining good connectivity with both the support and electrolyte layers. The anode thickness remains consistent at 21 μm across all samples, ensuring comparable electrochemical behavior. The microstructure reveals well-distributed Ni and YSZ phases with sufficient percolation for both electronic and ionic conduction.

The YSZ electrolyte layers exhibit dense, crack-free microstructures with excellent gas-tightness across all thickness variations. Cell_1 (7.05 μm) displays a uniform thin electrolyte with high density, Cell_2 (14.1 μm) maintains intermediate thickness while preserving structural integrity, and Cell_3 (21.2 μm) shows the thickest electrolyte configuration with maintained density. The absence of cracks or delamination confirms the effectiveness of the co-sintering process in achieving strong interfacial bonding.

The screen-printed LSCF cathode (22 μm) is visible as the topmost layer in all cells, showing a porous microstructure necessary for oxygen reduction and gas transport. The cathode appears well adhered to the electrolyte surface with good interfacial contact. The SEM analysis confirms successful fabrication of complete cells with varying electrolyte thicknesses while maintaining consistent other layer thicknesses, enabling a systematic study of electrolyte thickness effects on electrochemical performance.

Figure 3 presents the electrochemical impedance spectroscopy (EIS) results for all three NiFe-supported SOFC cells measured at operating temperatures of 700°C, 750°C, and 800°C. The Nyquist plots provide detailed insights into the individual resistance contributions and reveal the dominant factors affecting cell performance as a function of electrolyte thickness. The most striking observation from the EIS data is the dramatic scaling of total cell impedance with electrolyte thickness. Cell_1, with the thinnest electrolyte (7.05 μm electrolyte), exhibits the lowest overall impedance, with the real impedance (Z') extending to approximately 4.5 Ωcm² and imaginary impedance (Z'') reaching a maximum of ~1.2 Ωcm² at 700°C. In contrast, Cell_2 (14.1 μm electrolyte) shows intermediate impedance values with Z' ~ 12 Ωcm² and Z'' up to ~3 Ωcm², while Cell_3 (21.2 μm electrolyte) demonstrates the highest impedance with Z' reaching ~35 Ωcm² and Z'' up to ~12 Ωcm² under the same conditions.

The high-frequency intercept of each Nyquist plot corresponds to the ohmic resistance (R_O) of the cell, which is primarily determined by the ionic conductivity of the YSZ electrolyte. A clear correlation between electrolyte thickness and ohmic resistance is observed across all operating temperatures. At 800°C, the ohmic resistance increases from approximately 0.08 Ωcm² for Cell_1 to ~0.65 Ωcm² for Cell_2 and ~1.15 Ωcm² for Cell_3. This scaling is consistent with the expected linear relationship between electrolyte thickness and ionic resistance ($R = \varrho l/A$, where ϱ is resistivity, l is thickness, and A is area), confirming that the YSZ electrolyte represents the primary source of ohmic losses in these cells. The direct comparison of all three cells at 800°C (bottom-right panel) clearly illustrates the benefits of optimizing electrolyte thickness. Cell_1 demonstrates a total area-specific resistance (ASR) of approximately 1.1 Ωcm², compared to 3.4 Ωcm² for Cell_2 and 6.5 Ωcm² for Cell_3.

 doi:10.20944/preprints202603.1306.v1

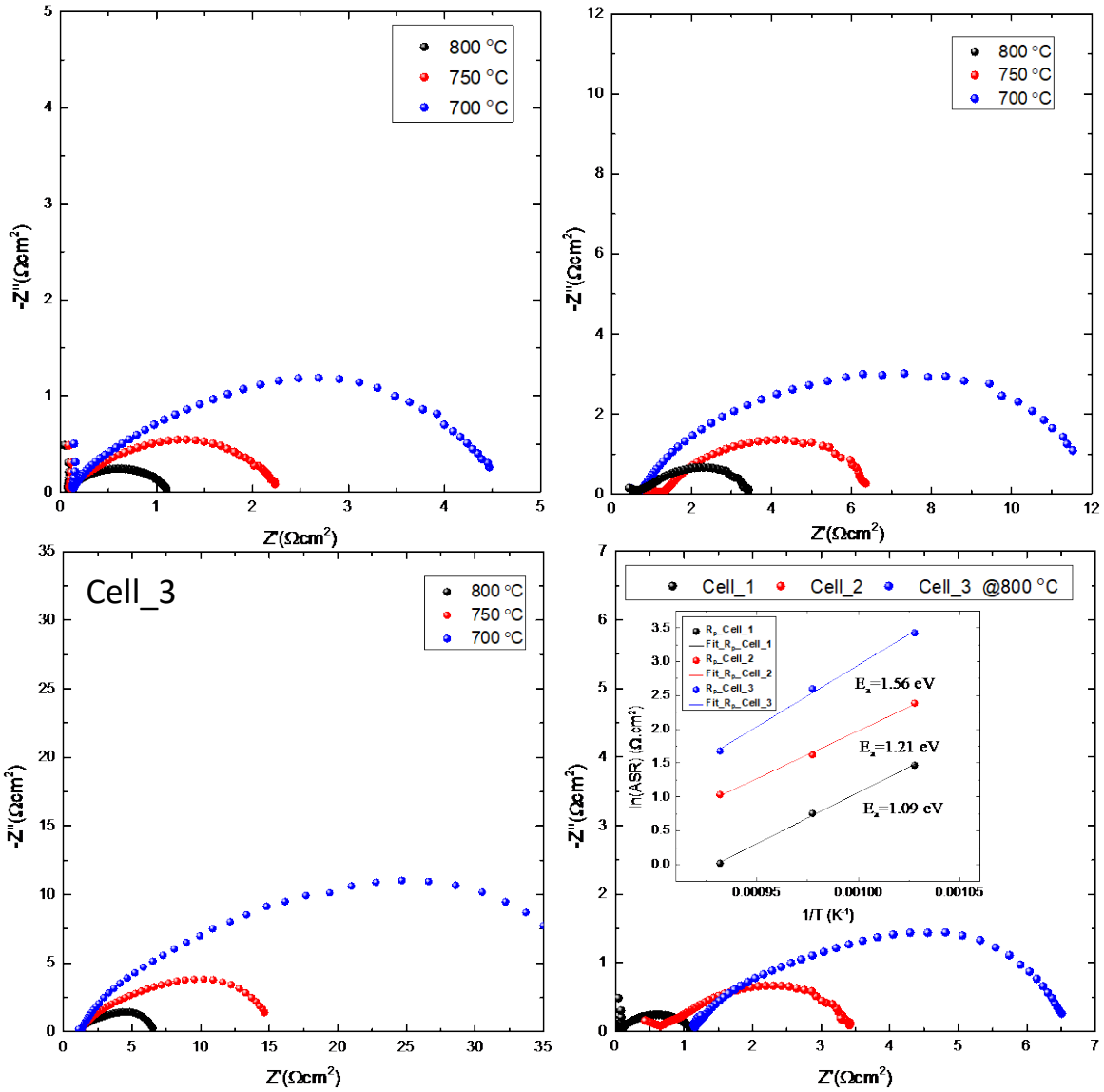

Figure 3. Electrochemical impedance spectroscopy (EIS) Nyquist plots for NiFe-supported SOFC cells with varying YSZ electrolyte thickness measured at 700°C, 750°C, and 800°C. The bottom right panel compares all cells at 800°C, demonstrating the dramatic reduction in total resistance achieved through electrolyte thickness optimization.

Arrhenius analysis of the total resistance (inset of the bottom-right panel) yields activation energies of 1.09, 1.21, and 1.56 eV for cells with electrolyte thicknesses of 7.05, 14.2, and 21.2 μm, respectively. For polycrystalline YSZ, the bulk (grain interior) activation energy is typically 0.85-0.90 eV, while grain boundary contributions add ~1.0-1.3 eV [11,33]. For the thinnest electrolyte (7.05 μm), the activation energy of 1.09 eV suggests predominantly bulk conduction with minimal grain boundary contribution. In contrast, Cell_3 (21.2 μm) exhibits 1.56 eV, indicating significant grain boundary resistance combined with enhanced polarization resistance due to current constriction effects at the electrode/electrolyte interface [10]. These interfacial effects particularly impact oxygen-ion incorporation kinetics [1], one of the rate-limiting elementary steps in the oxygen reduction reaction and gas diffusion. Thus, the systematic increase in total activation energy with electrolyte thickness can be attributed to two primary factors: (1) increased grain boundary resistance as thicker electrolytes contain more grain boundaries along the conduction path, and (2) enhanced polarization resistance, particularly affecting oxygen-ion incorporation kinetics at the electrode/electrolyte interface.

 doi:10.20944/preprints202603.1306.v1

The semicircular features in the Nyquist plots represent the combined electrode polarization resistances from both anode and cathode processes. Remarkably, the size and shape of these semicircles remain relatively consistent across all three cells when normalized for the different impedance scales. This observation indicates that the co-sintering fabrication process successfully maintained consistent electrode microstructures and electrochemical activity despite variations in electrolyte thickness.

The EIS analysis conclusively demonstrates that electrolyte thickness is the dominant factor determining overall cell resistance in this thickness range. The linear scaling of ohmic resistance with thickness, combined with minimal changes in electrode kinetics, indicates that further reduction of the electrolyte thickness below 7.05 μm could yield additional performance improvements, provided gas-tightness and mechanical integrity are maintained. These results establish clear design guidelines for optimizing MS-SOFC performance by systematically reducing electrolyte thickness while maintaining robust co-sintered interfaces.

Figure 4 presents the electrochemical performance characteristics of the three Ni-Fe supported SOFC cells, showing both current-voltage (I-V) curves and corresponding power density plots as a function of operating temperature. The results demonstrate a clear correlation between electrolyte thickness and cell performance across the entire temperature range investigated.

The performance follows the expected trend based on electrolyte thickness: Cell_1 > Cell_2 > Cell_3. At the highest operating temperature of 800°C, Cell_1 achieves a peak power density of approximately 0.32 W/cm² at a current density of ~0.4 A/cm², representing superior performance compared to the thicker electrolyte variants. Cell_2 demonstrates an intermediate peak power density of ~0.10 W/cm² at 800°C, while Cell_3 exhibits the lowest performance with a maximum power density of ~0.07 W/cm² under the same conditions. This represents approximately a 4.6-fold improvement in peak power density between the thinnest and thickest electrolyte configurations. The power density achieved by Cell_1 is competitive with MS-SOFC performance reported in the literature [38].

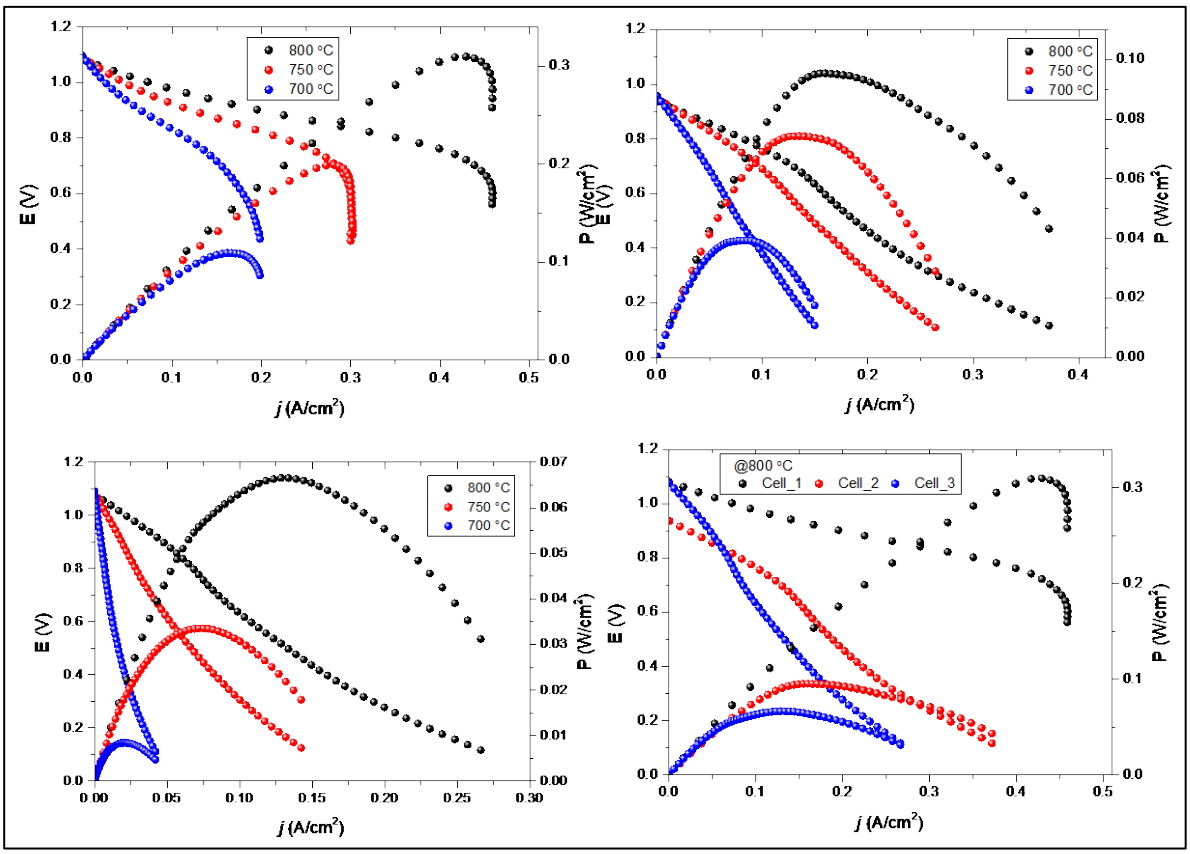

 doi:10.20944/preprints202603.1306.v1

Figure 4. Current-voltage (I-V) and power density characteristics of NiFe-supported SOFC cells with varying YSZ electrolyte thickness measured at 700°C, 750°C, and 800°C. Bottom right panel compares all cells at 800°C.

All cells exhibit the characteristic improvement in performance with increasing temperature, consistent with enhanced ionic conductivity and electrode kinetics at higher temperatures [22]. However, the magnitude of temperature sensitivity varies significantly with electrolyte thickness. Cell_1 maintains reasonable performance even at 700°C, achieving a peak power density of ~0.12 W/cm², while Cell_3 shows severely degraded performance at this lower temperature with peak power density dropping to ~0.02 W/cm². This temperature-sensitivity difference becomes particularly important for intermediate-temperature SOFC applications, where lower operating temperatures are desired to improve durability and system integration [31].

The power density curves reveal well-defined maxima for all cells, indicating optimal operating current densities that balance voltage and current to maximize power output. Cell_1 achieves peak power at current densities around 0.45 A/cm², compared to ~0.2 A/cm² for Cell_2 and ~0.12 A/cm² for Cell_3 at 800°C.

The direct comparison at 800°C (bottom right panel) provides a clear visualization of the performance hierarchy. The dramatic separation of the I-V curves demonstrates the substantial impact of electrolyte thickness optimization on practical cell performance. The voltage at any given current density follows the order Cell_1 > Cell_2 > Cell_3, which directly correlates with the impedance results and confirms that ohmic losses dominate the performance differences.

The I-V and power density results establish that electrolyte thickness optimization represents a critical design parameter for achieving high-performance MS-SOFCs. The 4.6-fold improvement in peak power density achieved through thickness reduction from 21.2 μm to 7.05 μm, combined with enhanced current-carrying capability and improved low-temperature performance, demonstrates the significant practical benefits obtainable through systematic electrolyte optimization in co-sintered metal-supported architectures.

Further, to understand the overall effect of electrolyte thicknesses on electrochemical performance, the Distribution of Relaxation Times (DRT) obtained from Electrochemical Impedance Spectroscopy (EIS) for three Ni-Fe supported SOFCs with varying electrolyte thicknesses (7.05, 14.2, and 21.2 μm) at 800 °C. Figure 5 presents the DRT results, revealing four distinct polarization processes (P_1-P_4) whose contributions vary systematically with electrolyte thickness. The DRT provides detailed insights into the distribution of different relaxation processes occurring within the cell, which are related to various resistance contributions, including ohmic resistance and electrode polarization.

High frequency peak P_1, attributed to ionic conduction through the YSZ electrolyte, based on its characteristic frequency range consistent with oxygen ion transport in YSZ [19,20]. This peak is weaker in Cell_1 (7.05 μm) but becomes increasingly prominent with thicker electrolytes, reaching maximum intensity in Cell_3 (21.2 μm). The significant growth of P_1 directly visualizes the increased ohmic resistance associated with increased electrolyte thickness, confirming that ionic transport resistance scales proportionally with the conduction path length [16].

The dominant medium-range frequency peak P_2 corresponds to charge transfer processes at the electrode/electrolyte interfaces, consistent with oxygen reduction reaction kinetics reported for Ni-YSZ/YSZ interfaces [19]. The systematic increase in P_2 magnitude with increasing electrolyte thickness can be attributed to current-constriction effects, where longer ion-conduction paths lead to a non-uniform current distribution at the interfaces [24].

 doi:10.20944/preprints202603.1306.v1

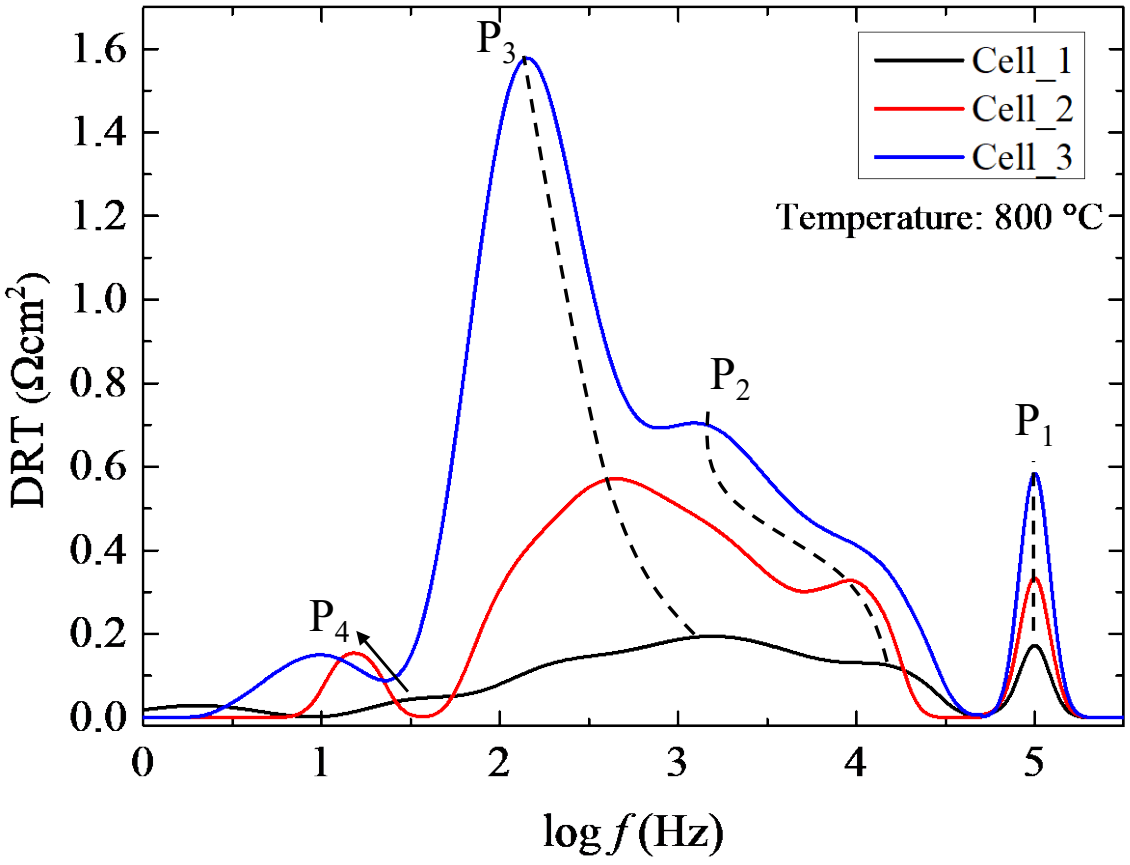

Figure 5. Distribution of Relaxation Times (DRT) from EIS for NiFe-supported SOFCs with varying YSZ electrolyte thicknesses.

Peak P_3 is assigned to oxygen-ion incorporation and exchange at triple-phase boundaries, a process well documented in SOFC electrode systems [2]. The relatively consistent magnitude of P_3 across all cells indicates that this fundamental electrochemical process is not significantly affected by variations in electrolyte thickness. The low-frequency contribution P_4 represents gas diffusion and conversion processes within the porous electrode structure [12,19]. The minimal variation of P_4 across cells confirms that electrode microstructure and gas transport pathways remain unaffected by electrolyte thickness.

Integration of the DRT peaks reveals that the total polarization resistance increase from Cell_1 to Cell_3 is dominated by the growth of P_1 (ohmic) and P_2 (charge transfer), while electrode-related processes (P_3, P_4) remain relatively constant. This quantitative deconvolution demonstrates that reducing YSZ thickness to ~7 μm effectively eliminates the high-frequency ohmic contribution while preserving electrode functionality, validating thin-electrolyte design strategies for high-performance MS-SOFCs.

4. Conclusions

This study systematically investigated the effect of YSZ electrolyte thickness on NiFe-supported SOFC performance using the co-sintering fabrication process. Microstructural analysis validated the co-sintering approach, producing dense, crack-free electrolyte layers with excellent interfacial bonding with other layers. EIS and DRT analysis confirmed that electrolyte ionic resistance dominates total cell impedance, scaling linearly with thickness, while electrode kinetics remained consistent across all cells. The thinnest electrolyte cell achieved a 4.6-fold higher peak power density (0.32 W/cm² at 800°C) than the thickest variant, primarily due to reduced ohmic resistance. The optimized cell demonstrated superior low-temperature performance, maintaining high power

 doi:10.20944/preprints202603.1306.v1

density even at 650°C, making it suitable for intermediate-temperature applications. This optimization study establishes that thin YSZ electrolytes (≤8 μm) maximize MS-SOFC performance while maintaining structural integrity, providing design guidelines for high-performance metal-supported fuel cell development with enhanced mechanical robustness for practical applications.

Acknowledgments: This research was supported by the National Research Foundation (NRF) of Korea, funded by the Korean government. (Ministry of Science and ICT(MSIT)) (No. RS-2023-00236572).

Conflicts of Interest: The authors have no relevant financial or non-financial interests to disclose.

Data Availability: Data will be made available on request.

References

1. S. Zarabi Golkhatmi, M. I. Asghar, and P. D. Lund, *Renewable and Sustainable Energy Reviews*, **161**, 112339 (2022).
2. S. Choi et al., *ACS Energy Lett.*, **9**, 4059–4067 (2024).
3. Z. Lin et al., *International Journal of Hydrogen Energy*, **142**, 180–185 (2025).
4. J. Li et al., *Advanced Energy and Sustainability Research*, **5**, 2400132 (2024).
5. N. Shah et al., *Journal of Power Sources*, **599**, 234211 (2024).
6. D. S. Dhawale, S. Biswas, G. Kaur, and S. Giddey, *Inorganic Chemistry Frontiers*, **10**, 6176–6192 (2023).
7. J. Li, Q. Cai, and B. A. Horri, *Materials Advances*, **6**, 39–83 (2025).
8. S. Jo et al., *Journal of the Korean Ceramic Society*, **57**, 135–151 (2020).
9. C. Ding and T. Hashida, *Energy Environ. Sci.*, **3**, 1729–1731 (2010).
10. S. Y. Shin, D.-K. Lim, T. Lee, and S.-Y. Jeon, *J. Electrochem. Sci. Technol*, **14**, 145–151 (2023).
11. S. Vafakhah, G. Kaur, and S. Giddey, *International Journal of Hydrogen Energy*, **111**, 833–847 (2025).
12. Z. D. Jin, M. K. Warshi, and H. J. Park, *Journal of Asian Ceramic Societies*, 1–8.
13. S. E. Wolf et al., *Journal of Materials Chemistry A*, **11**, 17977–18028 (2023).
14. Z. Zhang et al., *Automot. Innov.*, **8**, 443–471 (2025).
15. X. Wang et al., *Journal of Power Sources*, **277**, 474–479 (2015).
16. F. Capotondo et al., *Journal of Power Sources*, **613**, 234812 (2024).
17. S. E. Lee, J. S. Park, and H. J. Park, *Korean Journal of Metals and Materials*, **60**, 523–530 (2022).
18. Y.-W. Ju et al., *Journal of the Korean Ceramic Society*, **45**, 796.
19. N. A. Baharuddin et al., *International Journal of Energy Research*, **44**, 8296–8313 (2020).
20. D. Kim et al., *Journal of the Korean Ceramic Society*, **59**, 131–152 (2022).
21. J. W. Fergus, *Journal of Power Sources*, **162**, 30–40 (2006).
22. I. Danilenko et al., *Solid State Ionics*, **412**, 116581 (2024).
23. S. E. Lee, M. K. Warshi, and H. J. Park, *J. Mater. Chem. A* (2025).
24. J. Zhang, C. Lenser, N. H. Menzler, and O. Guillon, *Solid State Ionics*, **344**, 115138 (2020).
25. G. Zhang et al., *J Mater Sci: Mater Electron*, **34**, 1937 (2023).
26. S. H. Rahul et al., *ECS Trans.*, **57**, 857 (2013).
27. H. Shimada et al., *Ceramics International*, **44**, 3134–3140 (2018).
28. Y. F. Zhao, Z. D. Jin, S. E. Lee, and H. J. Park, *Ceramics International*, **51**, 4355–4365 (2025).
29. H. Sumi et al., *Sci Rep*, **11**, 10622 (2021).
30. X. Guo and R. Waser, *Progress in Materials Science*, **51**, 151–210 (2006).
31. M. J. Verkerk, B. J. Middelhuis, and A. J. Burggraaf, *Solid State Ionics*, **6**, 159–170 (1982).
32. J. Fleig, *Solid State Ionics*, **150**, 181–193 (2002).
33. S. B. Adler, *Chem. Rev.*, **104**, 4791–4844 (2004).
34. A. Talukdar et al., *International Journal of Energy Research*, **2024**, 6443247 (2024).
35. A. Leonide, V. Sonn, A. Weber, and E. Ivers-Tiffée, *J. Electrochem. Soc.*, **155**, B36 (2007).
36. S. E. Lee, M. K. Warshi, and H. J. Park, *J. Mater. Chem. A*, **13**, 33136–33146 (2025).
37. D. Klotz, A. Weber, and E. Ivers-Tiffée, *Electrochimica Acta*, **227**, 110–126 (2017).

 doi:10.20944/preprints202603.1306.v1

38. J. Nielsen and J. Hjelm, *Electrochimica Acta*, **115**, 31–45 (2014).
39. S. B. Adler, *Chem. Rev.*, **104**, 4791–4844 (2004).